

Subaru High- z Exploration of Low-Luminosity Quasars (SHELLQs). XXIV. 54 New Quasars and Candidate Obscured Quasars at $5.71 \leq z \leq 7.02$

YOSHIKI MATSUOKA,¹ KAZUSHI IWASAWA,² MASAFUSA ONUYE,^{3,4} TAKUMA IZUMI,⁵ MICHAEL A. STRAUSS,⁶ MASAYUKI AKIYAMA,⁷ KENTARO AOKI,⁸ JUNYA ARITA,⁹ XUHENG DING,^{10,4} MASATOSHI IMANISHI,^{5,11} NOBUNARI KASHIKAWA,⁹ TOSHIHIRO KAWAGUCHI,¹² SATOSHI KIKUTA,⁹ KOTARO KOHNO,^{13,14} CHIEN-HSIU LEE,¹⁵ TOHRU NAGAO,¹ CAMRYN L. PHILLIPS,⁶ MAHOSHI SAWAMURA,^{9,5} JOHN D. SILVERMAN,^{4,9,16,17} AYUMI TAKAHASHI,⁵ AND YOSHIKI TOBA^{18,19,1}

¹Research Center for Space and Cosmic Evolution, Ehime University, Matsuyama, Ehime 790-8577, Japan.

²ICREA and Institut de Ciències del Cosmos, Universitat de Barcelona, IEEC-UB, Martí i Franquès, 1, 08028 Barcelona, Spain.

³Waseda Institute for Advanced Study (WIAS), Waseda University, Shinjuku, Tokyo 169-0051, Japan.

⁴Kavli Institute for the Physics and Mathematics of the Universe, WPI, The University of Tokyo, Kashiwa, Chiba 277-8583, Japan.

⁵National Astronomical Observatory of Japan, Mitaka, Tokyo 181-8588, Japan.

⁶Department of Astrophysical Sciences, Princeton University, Peyton Hall, Princeton, NJ 08544, USA.

⁷Astronomical Institute, Tohoku University, Aoba, Sendai, 980-8578, Japan.

⁸Subaru Telescope, National Astronomical Observatory of Japan, Hilo, HI 96720, USA.

⁹Department of Astronomy, School of Science, The University of Tokyo, Tokyo 113-0033, Japan.

¹⁰School of Physics and Technology, Wuhan University, Wuhan 430072, China.

¹¹Department of Astronomical Science, Graduate University for Advanced Studies (SOKENDAI), Mitaka, Tokyo 181-8588, Japan.

¹²Graduate School of Science and Engineering, University of Toyama, Toyama, Toyama 930-8555, Japan.

¹³Institute of Astronomy, The University of Tokyo, Mitaka, Tokyo 181-0015, Japan.

¹⁴Research Center for the Early Universe, University of Tokyo, Tokyo 113-0033, Japan.

¹⁵Hobby-Eberly Telescope, McDonald Observatory, Fort Davis, TX 79734, USA.

¹⁶Center for Data-Driven Discovery, Kavli IPMU (WPI), UTIAS, The University of Tokyo, Kashiwa, Chiba 277-8583, Japan

¹⁷Center for Astrophysical Sciences, Department of Physics & Astronomy, Johns Hopkins University, Baltimore, MD 21218, USA

¹⁸Department of Physical Sciences, Ritsumeikan University, Kusatsu, Shiga 525-8577, Japan.

¹⁹Academia Sinica Institute of Astronomy and Astrophysics, Taipei 10617, Taiwan.

ABSTRACT

We present spectroscopic identification of 43 quasars and 11 candidate obscured quasars in the epoch of reionization (EoR) at $5.71 \leq z \leq 7.02$, along with 29 galaxies at similar redshifts. This is the 24th publication from the Subaru High- z Exploration of Low-Luminosity Quasars (SHELLQs) project, which exploits the Hyper Suprime-Cam (HSC) Subaru Strategic Program (SSP) imaging survey to search for EoR quasars. The HSC-SSP survey has completed, and this paper is likely the final installment of major (unobscured) quasar discoveries from the SHELLQs project. In addition to the EoR objects, we identified five strong [O III] line emitters at $z < 1$, 30 Galactic brown dwarfs, and 14 passive galaxies at $z \sim 2$, which contaminated our sample of photometric quasar candidates. The present paper focuses on describing the immediate outcome of the spectroscopic observations, while a statistical analysis of the full SHELLQs sample will be presented in our next publication.

1. INTRODUCTION

For more than 10 years, we have been carrying out a project to search for and characterize low-luminosity

quasars in the epoch of reionization (EoR, referring to $z > 5.6$ in this paper). The project, “Subaru High- z Exploration of Low-Luminosity Quasars (SHELLQs; Matsuoka et al. 2016)”, is based on the Subaru Strategic Program (SSP; Aihara et al. 2018) survey with Hyper Suprime-Cam (Miyazaki et al. 2018), a cutting-edge wide-field imager mounted at the prime focus of the Subaru Telescope. Candidate EoR quasars were selected

Corresponding author: Yoshiki Matsuoka
 matsuoka.yoshiki.ld@ehime-u.ac.jp

from the HSC images, mainly utilizing the i -, z -, and y -band photometry, with a Bayesian probabilistic algorithm (Mortlock et al. 2012) or simple color cuts. Spectroscopic identification of the candidates has been performed with the Subaru Telescope and the Gran Telescopio Canarias (GTC).

We have so far reported discovery of 139 broad-line (unobscured) quasars at $5.6 < z < 7.1$ in a series of publications (Matsuoka et al. 2016, 2018b,a, 2019a, 2022). The identified objects include the first known low-luminosity quasar at $z > 7$ (Matsuoka et al. 2019b) and the first confirmed pair of quasars at $z > 6$ (Matsuoka et al. 2024). The established sample was used to measure the quasar luminosity functions at $z = 6$ (Matsuoka et al. 2018c) and at $z = 7$ (Matsuoka et al. 2023), which indicated that quasars contribute only in a minor way to cosmic reionization. The black hole (BH) masses and Eddington ratios were estimated from the follow-up near-infrared (IR) spectroscopy (Onoue et al. 2019, 2021) or from the spectral shape around Ly α compared to low- z quasars (Takahashi et al. 2024). Observations with the Atacama Large Millimeter/submillimeter Array (ALMA) detected [C II] 158- μm line and far-IR continuum in many of the quasars (Izumi et al. 2018, 2019, 2021a,b; Sawamura et al. 2025), and revealed that the ratios between the host dynamical mass and BH mass are more or less consistent with the stellar-to-BH mass ratios measured in galaxies at $z \sim 0$.

Before the James Webb Space Telescope (JWST; Rigby et al. 2023) was launched, the SHELLQs quasars served as a unique statistical sample of the lowest-luminosity quasars or active galactic nuclei (AGNs) known in the EoR. Now with data from JWST, the SHELLQs sample is taking on a new role. Ding et al. (2023, 2025) observed 12 SHELLQs quasars with NIR-Cam, and achieved the first secure detection of starlight in hosts of EoR quasars. The same quasars were also observed with NIRSpec, allowing us to estimate BH masses as well as the star formation history in some of the objects with stellar absorption lines (Onoue et al. 2024, M. Onoue et al. 2025, in preparation). Related studies of the stellar-to-BH mass relation and the extended spectral properties are ongoing (e.g., J. D. Silverman et al. 2025, in preparation; C. L. Phillips et al. 2025, in preparation). In the meantime, JWST has revealed an abundant population of candidate low-luminosity AGNs in the EoR, which manifest as galaxies with broad Balmer lines or as “little red dots” (e.g., Onoue et al. 2023; Harikane et al. 2023; Kocevski et al. 2023, 2025; Matthee et al. 2024; Greene et al. 2024). The SHELLQs quasars occupy a unique luminosity range bridging

those new AGN candidates and classical quasars, and may represent the missing link between the two populations (Matsuoka et al. 2025).

The HSC-SSP survey completed its 330 nights of observation in 2021 December. The SHELLQs project continued spectroscopic identification of quasar candidates through 2025 March, and has now covered all primary candidates from the entire HSC-SSP dataset. This paper presents the results from all the spectroscopic observations since our last discovery paper (Matsuoka et al. 2022). This is likely the final installment of major (unobscured) quasar discoveries from the project, although discoveries of other populations, such as obscured quasars, may still continue (e.g., Kato et al. 2020; Iwamoto et al. 2025; Matsuoka et al. 2025). We plan to analyze the statistics of the full SHELLQs sample in the next paper (Y. Matsuoka et al. 2025, in preparation), and thus the present paper is kept short and concise. The sample and spectroscopic observations are presented in §2, and the results and short discussions appear in §3. A summary is given in §4. All magnitudes refer to point-spread function (PSF) magnitudes presented in the AB system (Oke & Gunn 1983) unless otherwise noted, corrected for Galactic extinction (Schlegel et al. 1998). We refer to z -band magnitudes with the AB subscript (“ z_{AB} ”), while redshift z appears without a subscript. The cosmological parameters are assumed to be $H_0 = 70 \text{ km s}^{-1} \text{ Mpc}^{-1}$, $\Omega_M = 0.3$, and $\Omega_\Lambda = 0.7$.

2. OBSERVATIONS

The candidates presented here were selected from the S21A and S23B internal data releases (DRs) of the HSC-SSP. The latter is equivalent to the final public DR of the survey, which will take place in the near future. In Matsuoka et al. (2022) and earlier papers, quasar candidates were limited to those with $\mu/\mu_{\text{PSF}} < 1.2$ in the z band (for i -band dropouts, which are $z \sim 6$ quasar candidates) or with $\mu/\mu_{\text{PSF}} < 3.0$ in the y band (for z -band dropouts, $z \sim 7$ quasar candidates). Here, μ and μ_{PSF} represent the image adaptive moments of a source and its PSF model, respectively. We have tested a relaxed shape condition since then, and as a result, the present paper includes more extended i -dropouts with $\mu/\mu_{\text{PSF}} < 3.0$ in the z band. All the other selection criteria are identical to those described in our past publications (e.g., Matsuoka et al. 2022). We consistently applied updated selection criteria to all previous imaging data (reprocessed with the latest pipeline), and as a result, the current candidates are distributed across the entire 1100-deg 2 area of the completed HSC-SSP footprint.

Table 2 in the Appendix presents the journal of spectroscopic observations for a total of 132 candidates. At the Subaru Telescope, we used the Faint Object Camera and Spectrograph (FOCAS; Kashikawa et al. 2002) to cover the red-optical wavelengths from 0.75 to 1.0 μm . We used the VPH900 grism and 1''.0 slit, which provide a spectral resolution of $R \sim 1200$. All the observations have been carried out in the classical mode, with the program IDs of S18B-011I, S22A-025, S22B-042, S24A-053, and S24B-025. At the GTC, all the observations have been conducted in the queue mode. The program IDs are GTC42-21B, GTC30-22A, GTC23-24A, and GTC3-24B. We used the Optical System for Imaging and low-intermediate-Resolution Integrated Spectroscopy (OSIRIS; Cepa et al. 2000). The R2500I grism was used with the 1''.0 longslit, giving a spectral coverage from 0.75 to 1.0 μm at a resolution of $R \sim 1500$.

3. RESULTS AND DISCUSSION

Figures 1 – 3 present the reduced spectra of 43 candidates that turned out to be quasars at $z = 5.71 - 7.02$. They are characterized by broad Ly α line and/or blue continuum emission, as well as the sharp spectral break due to the H I absorption by the intergalactic medium. Some of the spectra are severely affected by the noise from sky emission, especially at the redder part, where there are strong sky lines and the detector sensitivity is relatively low. The spiky features at 9300 – 9500 Å in $J133013.00 + 423432.2$ and $J140344.28 + 423114.3$ are due to sky noise. We also found 11 high- z objects with very luminous and narrow Ly α emission (Figure 4), with line luminosities $L_{\text{Ly}\alpha} > 10^{43}$ erg s $^{-1}$ and full widths at half maximum (FWHMs) < 500 km s $^{-1}$ after correcting for the instrumental resolution. Our past publications (Matsuoka et al. 2016, 2018b,a, 2019a, 2022) have consistently classified such objects as “candidate obscured (narrow-line) quasars”, since Ly α emitters at lower redshifts are known to be dominated by AGNs at $L_{\text{Ly}\alpha} > 10^{43}$ erg s $^{-1}$ (e.g., Konno et al. 2016; Sobral et al. 2018; Spinosa et al. 2020). Indeed, we observed 11 targets (out of 34 known at that time) from this population with JWST/NIRSpec in Cycles 1 and 2, and found that seven of them exhibit broad H I Balmer lines and He I lines, indicating that they are mildly-obscured quasars (Matsuoka et al. 2025). $J020719.59 + 023826.0$ and $J142322.01 + 020612.8$ reported in this paper were included among the JWST targets, and both of them have broad rest-optical lines.

Galaxies at similar redshifts without strong Ly α emission ($L_{\text{Ly}\alpha} < 10^{43}$ erg s $^{-1}$) are presented in Figures 5 – 6. Among them, $J140637.84 + 430623.2$ and $J140625.39 + 430504.7$ were found within a single cir-

pular FOCAS field-of-view with a diameter of 6 arcmin. The galaxies are at the identical redshift of $z = 5.98$, and their angular separation (2.6 arcmin) corresponds to 900 kpc in projected proper distance. The presence of two such luminous galaxies ($M_{1450} = -23.3$ and -22.3) in close proximity suggests the possibility of a galaxy overdensity in this region. Additional spectroscopy of surrounding fainter galaxies would be required to test this possibility (e.g., Toshikawa et al. 2012).

We note that the separation between quasars and galaxies is not always straightforward, especially when Ly α is weak or absent. Following our previous papers (e.g., Matsuoka et al. 2016), we classified objects with a hint of broad spectral bump around Ly α as quasars, and the remaining objects as galaxies. The line and continuum properties of the EoR objects described above (quasars, candidate obscured quasars, and galaxies) were measured as in Matsuoka et al. (2018b), and are listed in Table 1.

Our quasar candidates also included a significant number of interlopers at lower redshifts. Figure 7 shows galaxies with strong [O III] $\lambda 4959$ and $\lambda 5007$ emission lines at $0.7 < z < 1.0$. The [O III] lines are covered by the HSC z band, and the broad-band colors of these objects mimic Ly α of quasars at $z \sim 6$. Their line properties are listed at the bottom of Table 1. Finally, we identified 44 sources with red continuum without a sharp break. The 30 objects in Figures 8 – 9 are point sources with our definition of $\mu/\mu_{\text{PSF}} < 1.2$, and are most likely Galactic brown dwarfs. Following our previous papers, we estimated their spectral types by fitting the spectral standard templates of M4- to T8-type dwarfs (Burgasser 2014; Skrzypek et al. 2015) to the observed spectra. The best-fit types are indicated in the individual panels of the figure. On the other hand, the 14 objects in Figure 10 have more extended shape with $\mu/\mu_{\text{PSF}} > 1.2$. It is known that passive galaxies at $z = 1 - 2$ contaminate high- z quasar selection, if extended sources are not removed effectively (e.g., Euclid Collaboration et al. 2019). Indeed, we found that the spectra of the 14 extended objects are fitted reasonably well with a spectral template of a passive galaxy (Coleman et al. 1980) with the best-fit redshifts of $z = 1.5 - 2.2$. The redshift estimates are very uncertain, because of the limited spectral coverage and data quality.

For the same reason, the separation between Galactic brown dwarfs and passive galaxies remains somewhat ambiguous. As a test, we fitted the templates of brown dwarfs and a passive galaxy to all the 44 objects with red continuum, and found that (i) a passive galaxy template is favored by only one of the 30 point sources and (ii) brown dwarf templates are favored by only three of the

14 extended sources, based on the reduced χ^2 values. This gives us some confidence that the separation between brown dwarfs and passive galaxies is broadly correct, although we cannot rely too heavily on the classification of individual objects. Near-IR photometry would be useful to clearly separate the two contaminating populations, but such an analysis is beyond the scope of this paper.

4. SUMMARY

This is the 24th publication of the SHELLQs project. The HSC-SSP survey completed its 330 nights of observation in 2021 December, and here we show the immediate results from the follow-up spectroscopy carried out between 2021 November and 2025 March. This paper is likely the final installment of major (unobscured) quasar discoveries from the project. We present 132 spectra of photometric quasar candidates, which include 43 quasars at $5.71 \leq z \leq 7.02$, 11 candidate obscured (narrow-line) quasars at $6.01 \leq z \leq 6.88$, and 29 galaxies without strong Ly α emission at similar redshifts. The two galaxies $J140637.84 + 430623.2$ and $J140625.39 + 430504.7$ are separated by 900 kpc in projected proper distance and have identical redshifts ($z = 5.98$), which may indicate the presence of a galaxy overdensity in this region. The remaining candidates included five galaxies with strong [O III] lines at $0.7 < z < 1.0$, 30 Galactic brown dwarfs, and 14 passive galaxies at $1.5 < z < 2.2$, although the separation between the latter two classes remains somewhat ambiguous, given the quality of our spectra. We are currently working on a statistical analysis of the full SHELLQs sample, which will be presented in our next publication (Y. Matsuoka et al. 2025, in preparation).

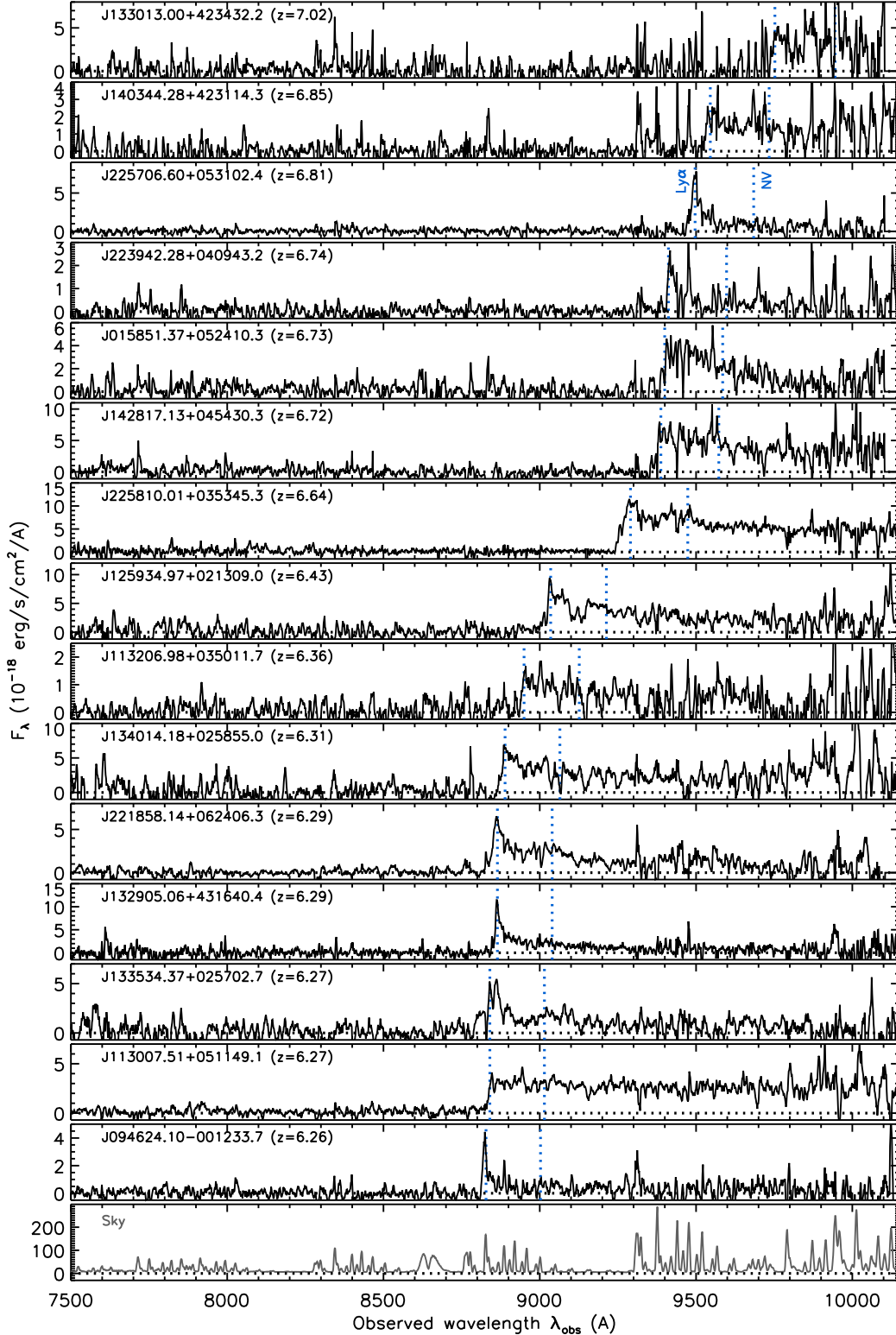


Figure 1. Discovery spectra of the first set of 15 quasars, displayed in decreasing order of redshift. The object name and the estimated redshift (with uncertainty $\Delta z \sim 0.01 - 0.1$; Matsuoka et al. 2022) are indicated at the top left corner of each panel. The blue dotted lines mark the expected positions of the Ly α and N V $\lambda 1240$ emission lines, given the redshifts. The spectra were smoothed using inverse-variance weighted means over 3 – 9 pixels (depending on the signal-to-noise ratio), for display purposes. The bottom panel displays a sky spectrum, as a guide to the expected noise.

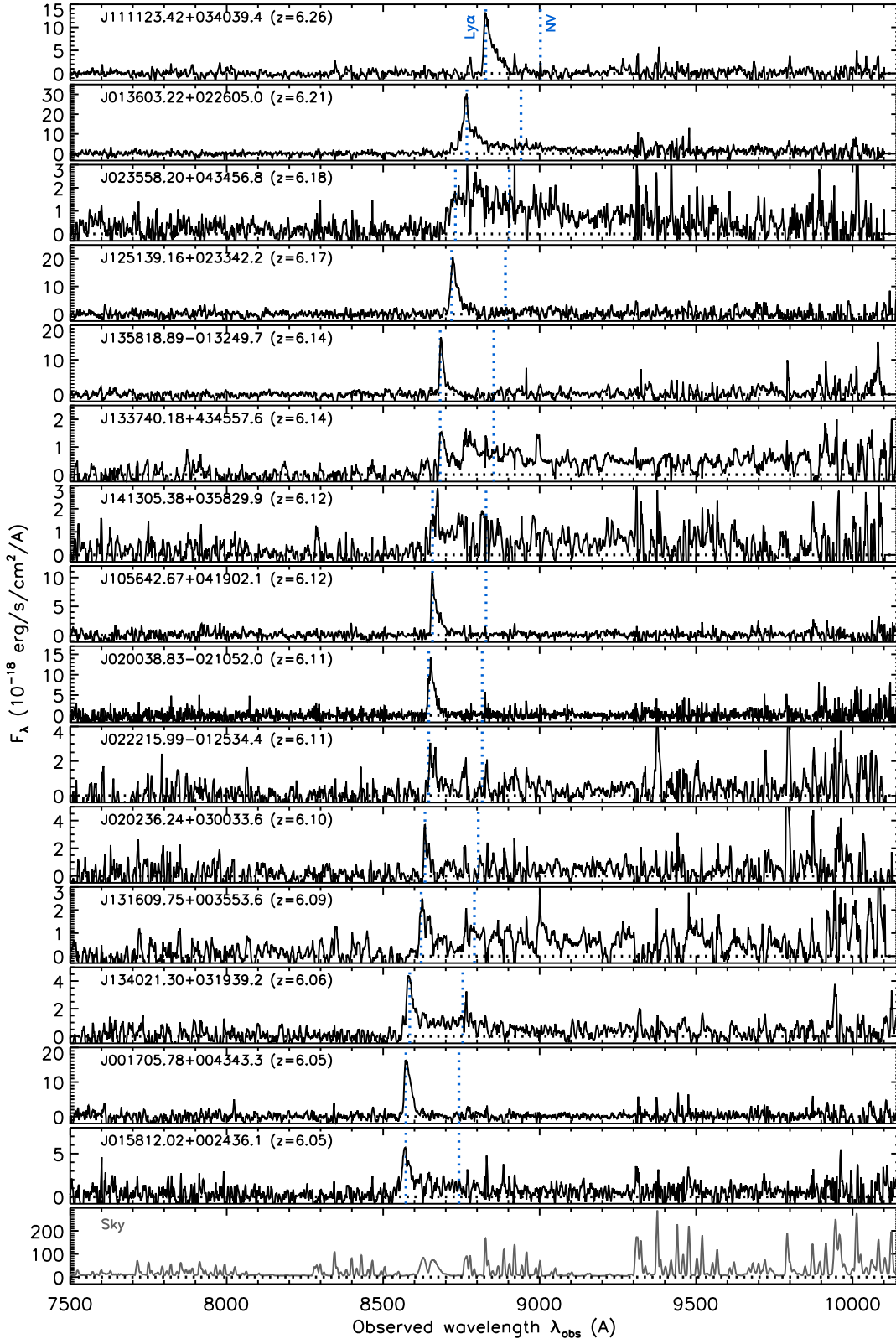


Figure 2. Same as Figure 1, but for the second set of 15 quasars.

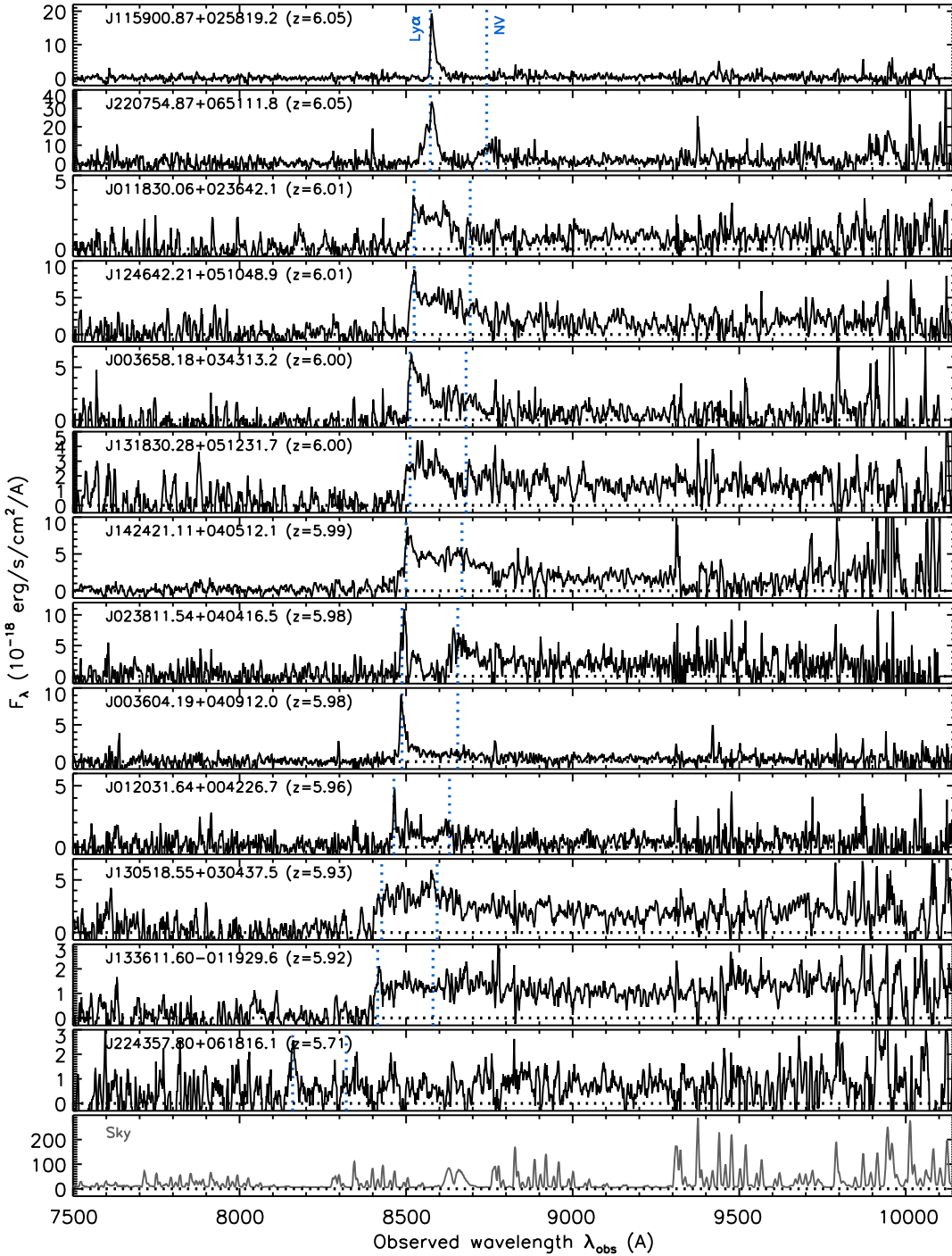


Figure 3. Same as Figure 1, but for the third set of 13 quasars.

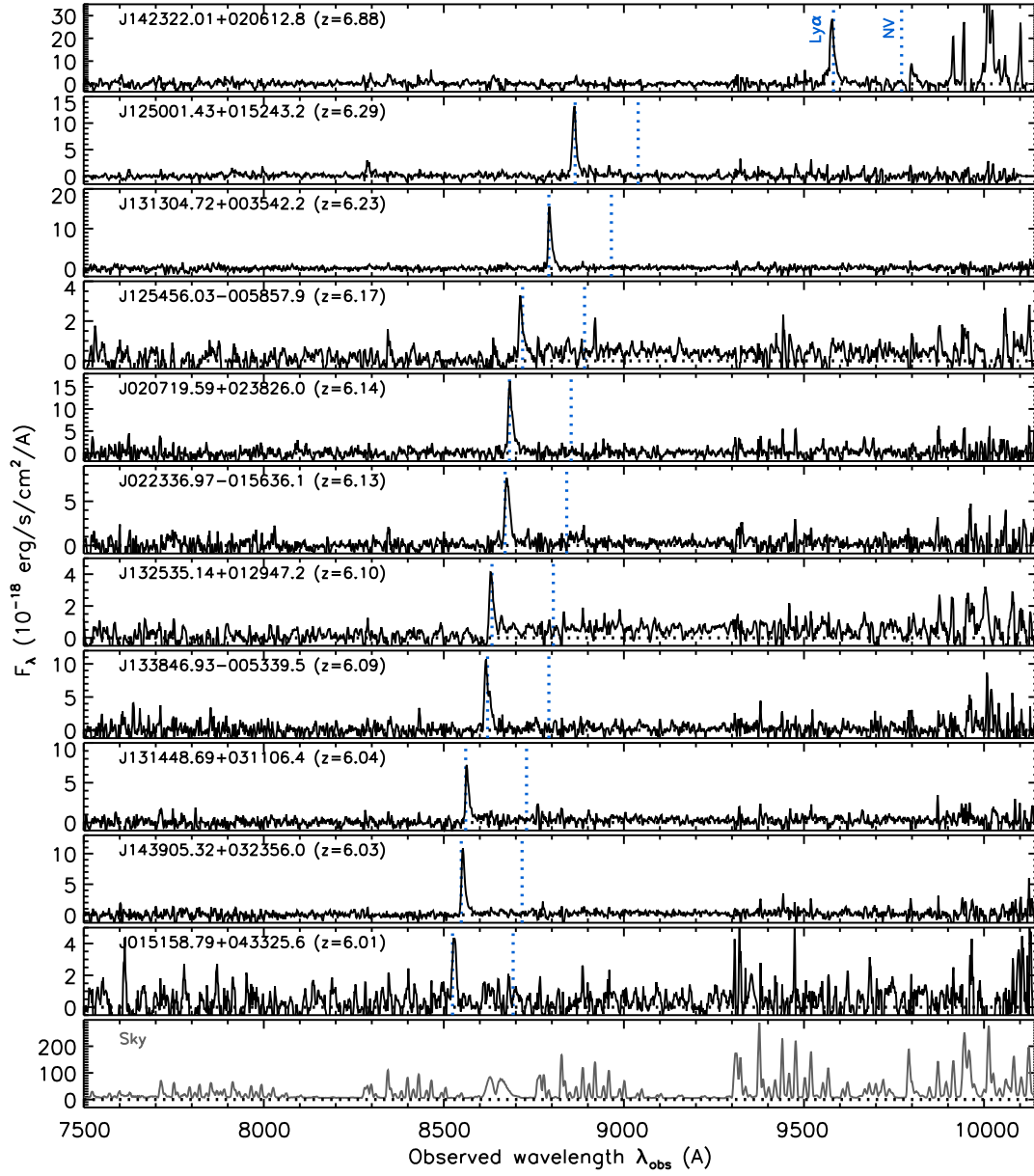


Figure 4. Same as Figure 1, but for 11 candidate obscured (narrow-line) quasars.

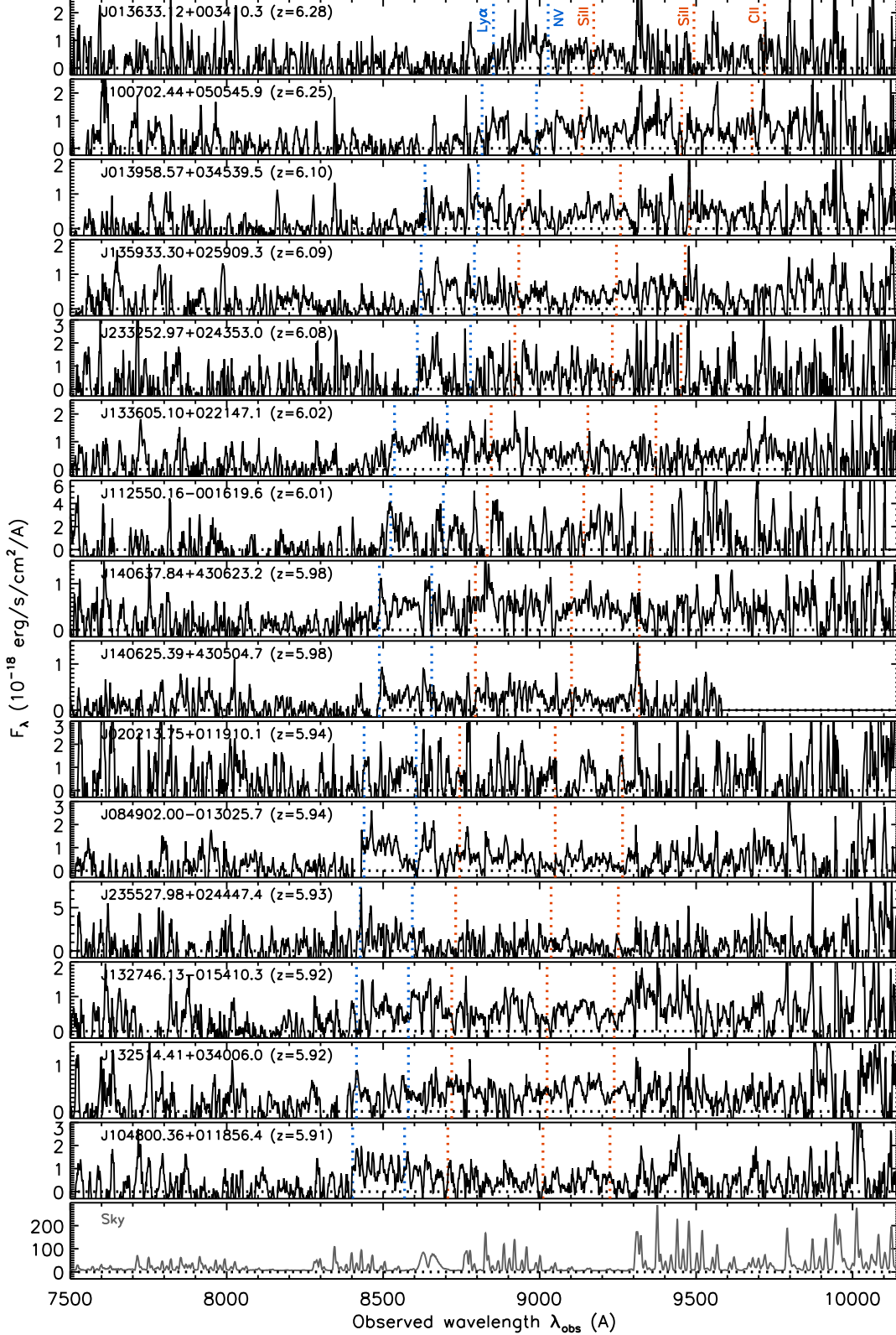


Figure 5. Same as Figure 1, but for the first set of 15 galaxies. The expected positions of Si II $\lambda 1260$, Si II $\lambda 1304$, and C II $\lambda 1335$ are marked by the red dotted lines. The flux excess at ~ 8780 Å in J013633.12 + 003410.3 is due to sky noise (see the bottom panel).

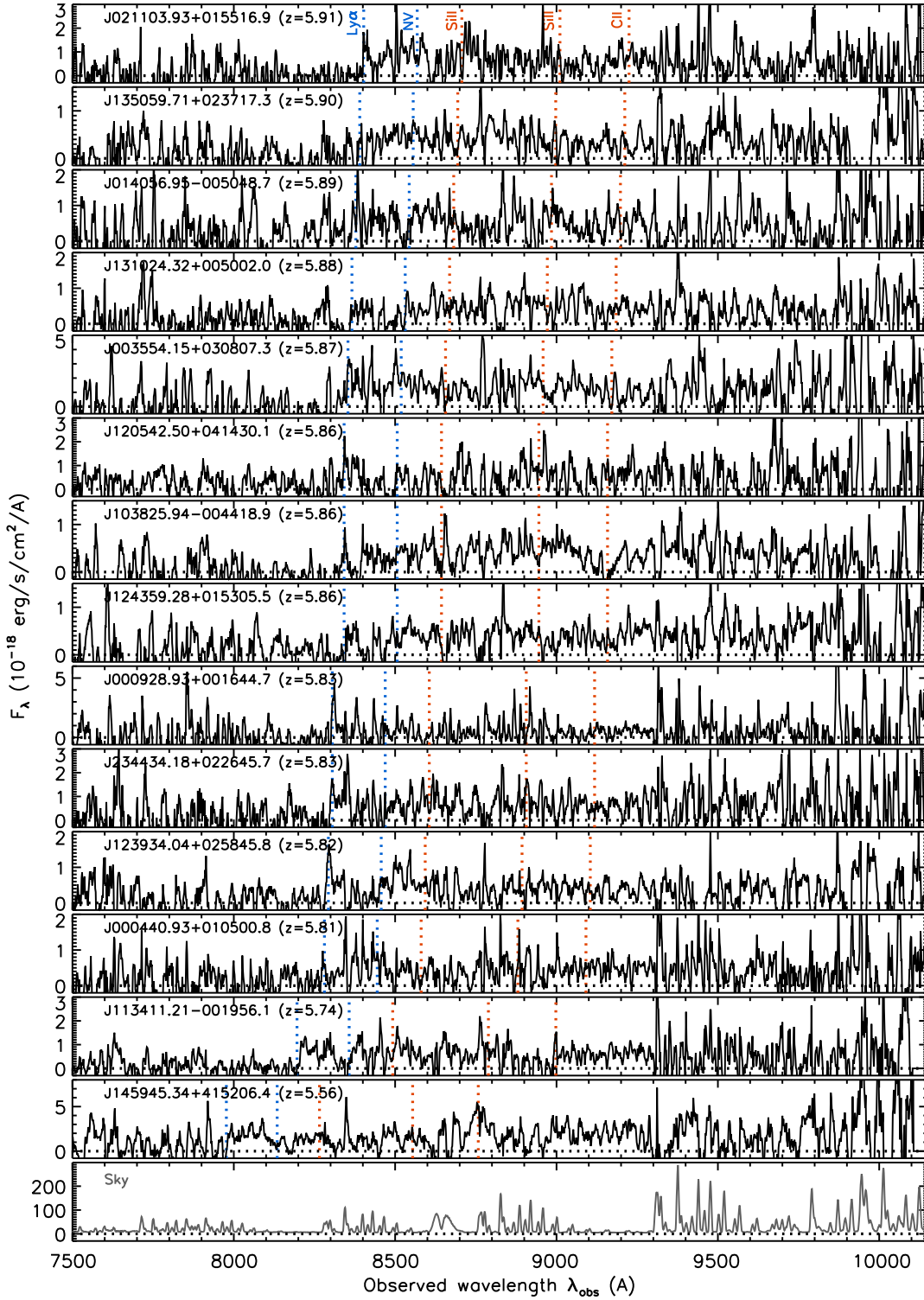


Figure 6. Same as Figure 5, but for the second set of 14 galaxies.

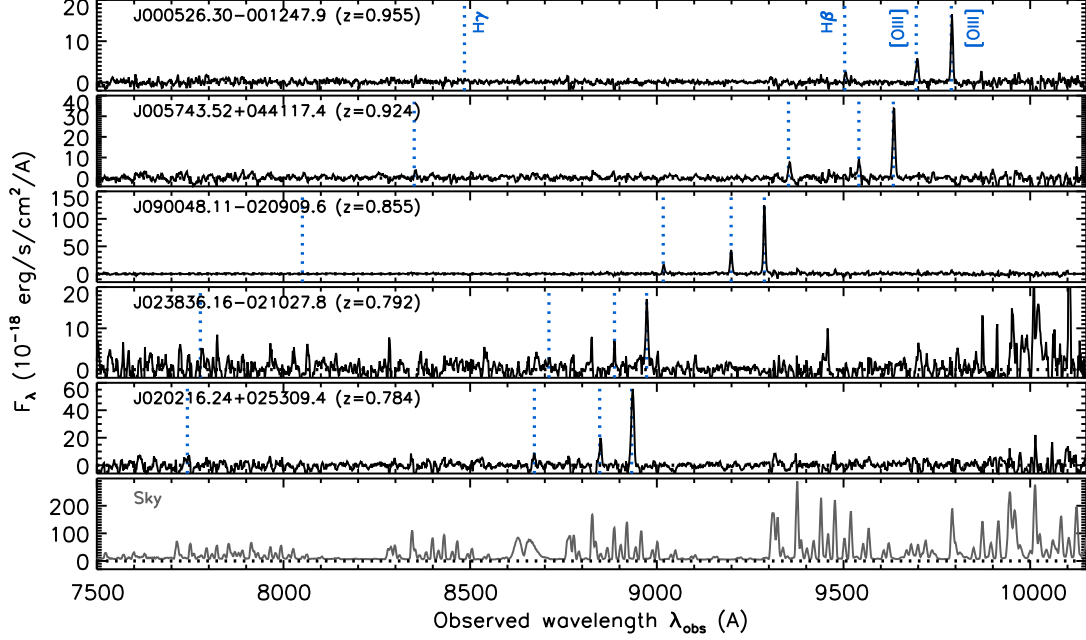


Figure 7. Same as Figure 1, but for five galaxies with strong [O III] $\lambda 4959$ and $\lambda 5007$ lines at $0.7 < z < 1.0$. The blue dotted lines mark the expected positions of the $H\gamma$, $H\beta$, and [O III] $\lambda 4959$, $\lambda 5007$ emission lines, given the redshifts.

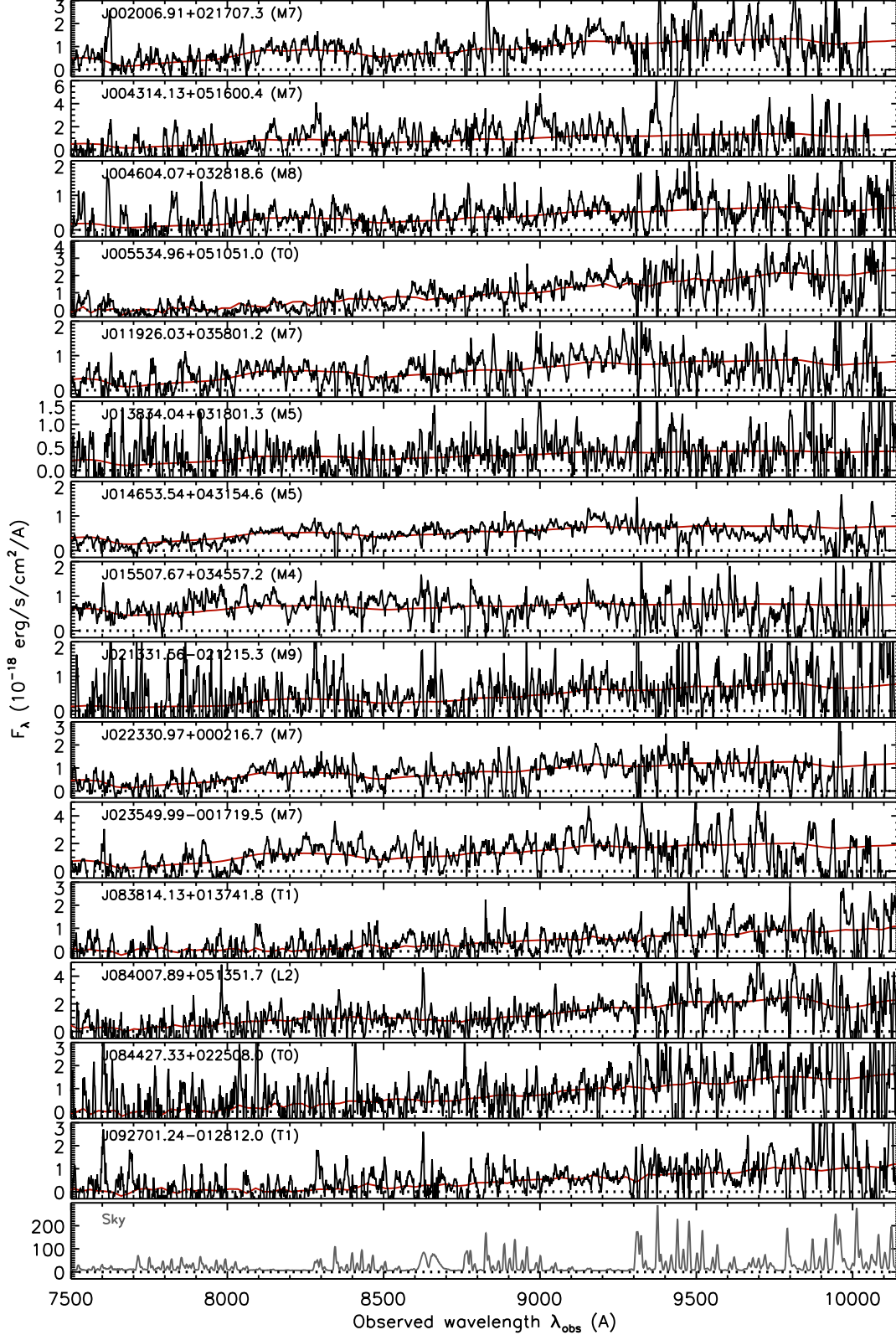


Figure 8. Same as Figure 1, but for the first set of 15 brown dwarfs, ordered by the right ascension. The red lines represent the best-fit templates, whose spectral types are indicated at the top left corner of the individual panels.

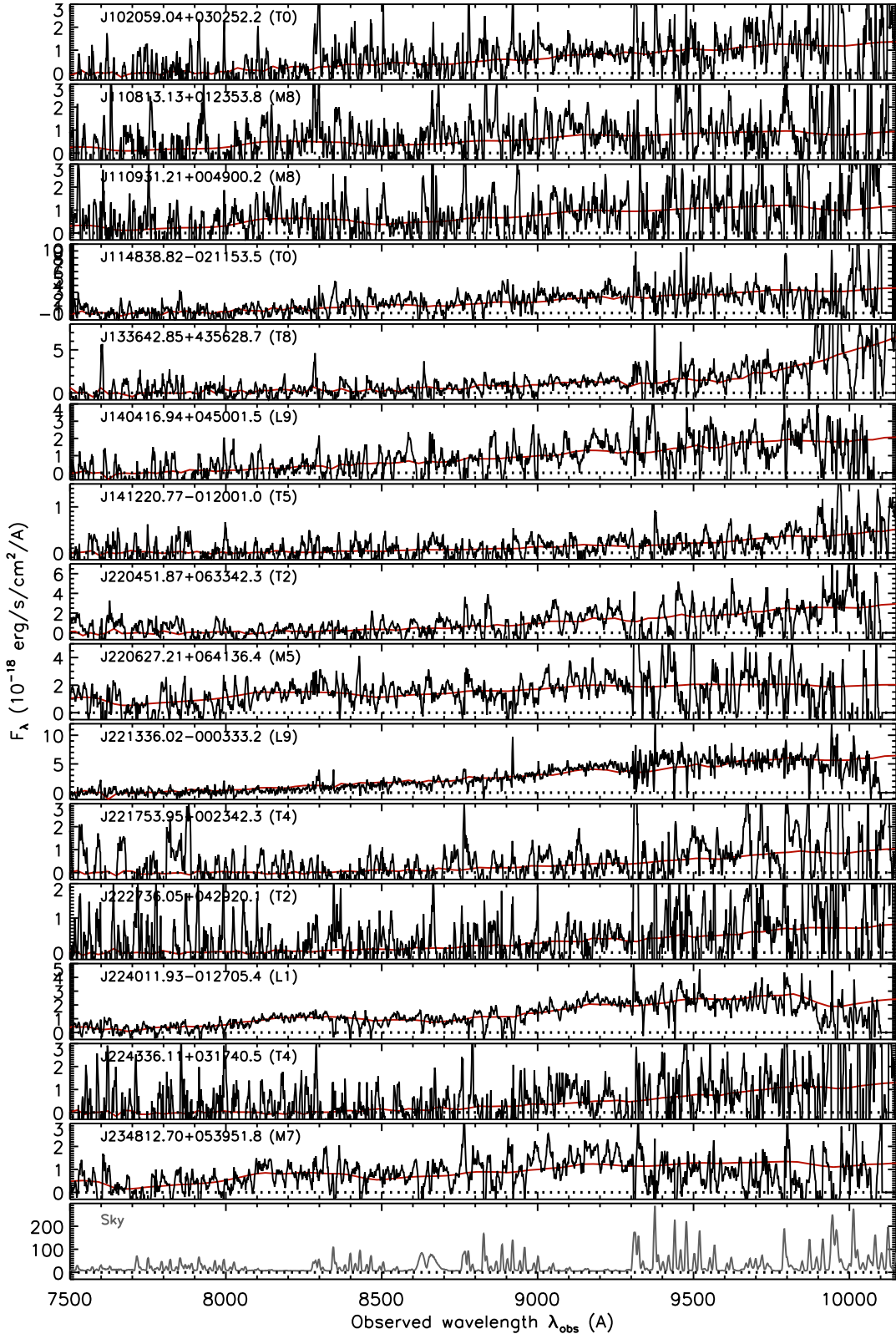


Figure 9. Same as Figure 8, but for the second set of 15 brown dwarfs.

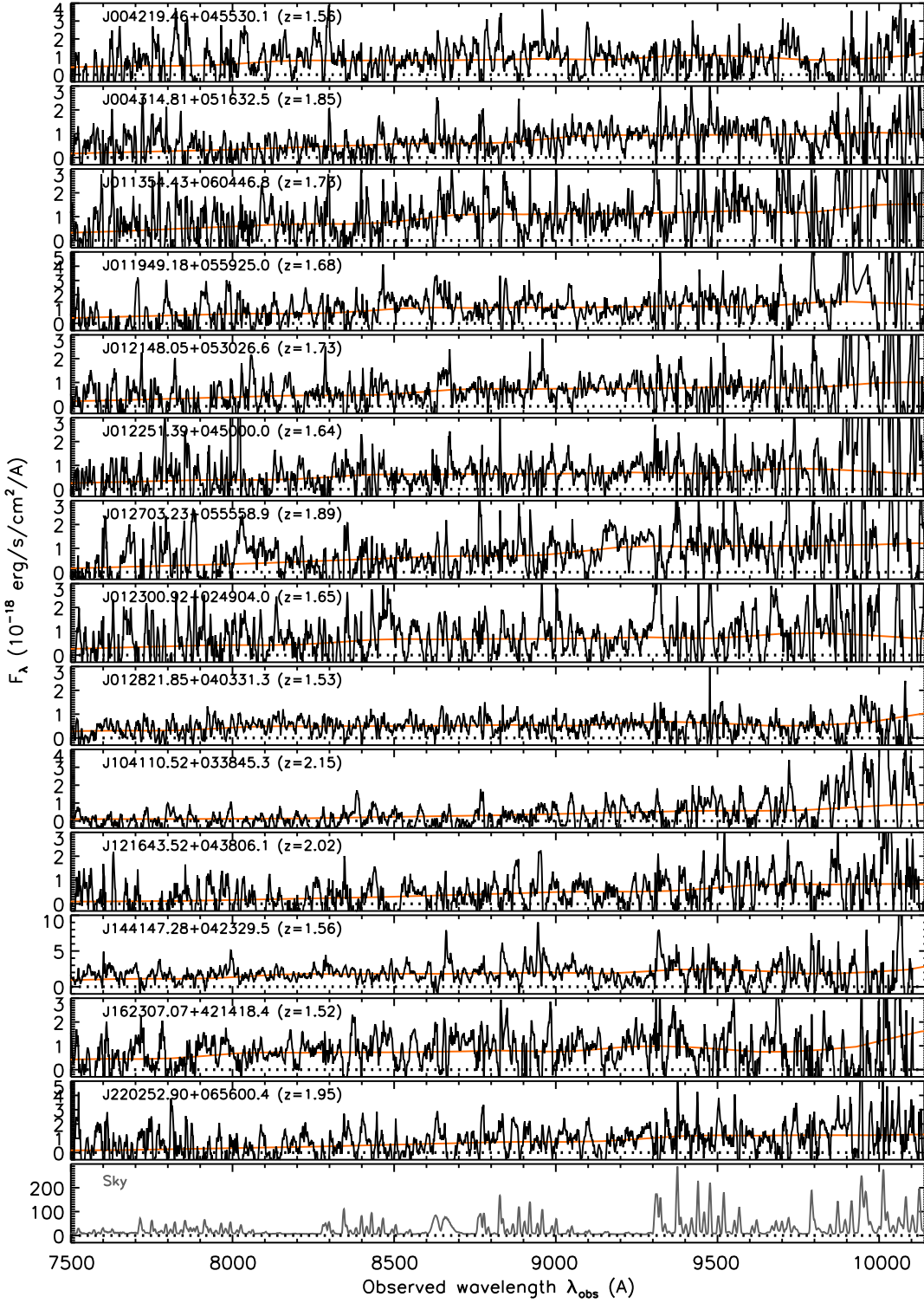


Figure 10. Same as Figure 1, but for 14 passive galaxies at $1.5 < z < 2.2$. The orange lines represent the best-fit templates, with the inferred redshifts indicated at the top left corner of the individual panels. The χ^2 values indicate the redshift errors up to $\Delta z = 0.03$, but the redshifts are likely more uncertain, since the fitting uses only a single template spectrum. For more complicated modeling, we would need higher quality data over wider spectral coverage.

Table 1. Spectroscopic Properties

Name	Redshift	M_{1450}	Line	EW_{rest}	FWHM	$\log L_{\text{line}}$
		(mag)		(Å)	(km s $^{-1}$)	(L_{line} in erg s $^{-1}$)
Quasars						
<i>J133013.00 + 423432.2</i>	7.02	-25.58 ± 0.21
<i>J140344.28 + 423114.3</i>	6.85	-24.45 ± 0.11	Ly α	8 ± 2	1700 ± 1000	43.56 ± 0.11
<i>J225706.60 + 053102.4</i>	6.81	-23.87 ± 0.18	Ly α	41 ± 9	940 ± 430	44.06 ± 0.06
<i>J223942.28 + 040943.2</i>	6.74	-23.07 ± 0.13	Ly α	13 ± 2	480 ± 140	43.24 ± 0.03
<i>J015851.37 + 052410.3</i>	6.73	-23.92 ± 0.53	Ly α	100 ± 60	11000 ± 4000	44.45 ± 0.12
<i>J142817.13 + 045430.3</i>	6.72	-25.71 ± 0.08
<i>J225810.01 + 035345.3</i>	6.64	-26.10 ± 0.01	Ly α	13 ± 1	3000 ± 1200	44.43 ± 0.02
<i>J125934.97 + 021309.0</i>	6.43	-24.99 ± 0.06	Ly α	31 ± 3	6300 ± 900	44.37 ± 0.03
<i>J113206.98 + 035011.7</i>	6.36	-23.56 ± 0.08
<i>J134014.18 + 025855.0</i>	6.31	-24.99 ± 0.07	Ly α	17 ± 3	1100 ± 1300	44.11 ± 0.06
<i>J221858.14 + 062406.3</i>	6.29	-24.31 ± 0.11	Ly α	20 ± 3	1900 ± 600	43.92 ± 0.05
<i>J132905.06 + 431640.4</i>	6.29	-23.87 ± 0.10	Ly α	95 ± 11	2000 ± 2100	44.40 ± 0.03
<i>J133534.37 + 025702.7</i>	6.27	-24.20 ± 0.07	Ly α	15 ± 2	2300 ± 300	43.76 ± 0.05
<i>J113007.51 + 051149.1</i>	6.27	-25.16 ± 0.02
<i>J094624.10 - 001233.7</i>	6.26	-22.99 ± 0.14	Ly α	21 ± 4	440 ± 630	43.43 ± 0.05
<i>J111123.42 + 034039.4</i>	6.26	-22.46 ± 0.19	Ly α	260 ± 50	660 ± 110	44.30 ± 0.01
<i>J013603.22 + 022605.0</i>	6.21	-24.46 ± 0.15	Ly α	95 ± 14	670 ± 390	44.66 ± 0.02
<i>J023558.20 + 043456.8</i>	6.18	-23.65 ± 0.10	Ly α	41 ± 8	5000 ± 3300	43.95 ± 0.07
<i>J125139.16 + 023342.2</i>	6.17	-21.53 ± 0.94	Ly α	780 ± 670	780 ± 220	44.41 ± 0.01
<i>J135818.89 - 013249.7</i>	6.14	-22.18 ± 0.64	Ly α	200 ± 120	430 ± 130	44.07 ± 0.02
<i>J133740.18 + 434557.6</i>	6.14	-23.11 ± 0.05	Ly α	6 ± 1	710 ± 200	42.93 ± 0.04
<i>J141305.38 + 035829.9</i>	6.12	-23.46 ± 0.11
<i>J105642.67 + 041902.1</i>	6.12	-21.59 ± 0.31	Ly α	270 ± 80	550 ± 380	43.98 ± 0.01
<i>J020038.83 - 021052.0</i>	6.11	-21.43 ± 0.30	Ly α	420 ± 120	700 ± 130	44.08 ± 0.01
<i>J022215.99 - 012534.4</i>	6.11	-22.66 ± 0.13	Ly α	29 ± 5	1200 ± 1100	43.42 ± 0.06
<i>J020236.24 + 030033.6</i>	6.10	-23.29 ± 0.09	Ly α	10 ± 2	800 ± 480	43.21 ± 0.08
<i>J131609.75 + 003553.6</i>	6.09	-23.51 ± 0.14	Ly α	9 ± 3	1300 ± 700	43.24 ± 0.13
<i>J134021.30 + 031939.2</i>	6.06	-22.87 ± 0.11	Ly α	64 ± 7	3400 ± 1600	43.85 ± 0.02
<i>J001705.78 + 004343.3</i>	6.05	-21.91 ± 0.32	Ly α	410 ± 120	790 ± 90	44.25 ± 0.01
<i>J015812.02 + 002436.1</i>	6.05	-23.33 ± 0.07	Ly α	61 ± 5	4200 ± 1700	44.01 ± 0.02
<i>J115900.87 + 025819.2</i>	6.05	-22.82 ± 0.08	Ly α	600 ± 530	430 ± 30	44.17 ± 0.01
<i>J220754.87 + 065111.8</i>	6.05	-24.44 ± 0.08	Ly α	84 ± 7	1100 ± 100	44.60 ± 0.01
<i>J220754.87 + 065111.8</i>	NV	33 ± 4	1800 ± 600	44.20 ± 0.03
<i>J011830.06 + 023642.1</i>	6.01	-23.70 ± 0.04	Ly α	32 ± 3	6100 ± 1700	43.88 ± 0.03
<i>J124642.21 + 051048.9</i>	6.01	-24.37 ± 0.06	Ly α	61 ± 5	7800 ± 900	44.43 ± 0.02
<i>J003658.18 + 034313.2</i>	6.00	-23.29 ± 0.12	Ly α	100 ± 10	2400 ± 200	44.22 ± 0.02
<i>J131830.28 + 051231.7</i>	6.00	-24.26 ± 0.05	Ly α	16 ± 2	4700 ± 600	43.82 ± 0.04

Table 1 *continued*

Table 1 (*continued*)

Name	Redshift	M_{1450}	Line	EW_{rest}	FWHM	$\log L_{\text{line}}$
		(mag)		(Å)	(km s $^{-1}$)	(L_{line} in erg s $^{-1}$)
<i>J142421.11 + 040512.1</i>	5.99	-24.53 ± 0.03	Ly α	56 ± 3	10000 ± 1000	44.45 ± 0.02
<i>J023811.54 + 040416.5</i>	5.98	-24.67 ± 0.09	Ly α	6 ± 1	300 ± 300	43.57 ± 0.05
<i>J003604.19 + 040912.0</i>	5.98	-23.05 ± 0.07	Ly α	88 ± 7	750 ± 110	44.05 ± 0.02
<i>J012031.64 + 004226.7</i>	5.96	-23.08 ± 0.08	Ly α	53 ± 6	2900 ± 1100	43.84 ± 0.04
<i>J130518.55 + 030437.5</i>	5.93	-24.52 ± 0.05
<i>J133611.60 - 011929.6</i>	5.92	-23.94 ± 0.03	Ly α	0.4 ± 0.4	560 ± 290	42.07 ± 0.39
<i>J224357.80 + 061816.1</i>	5.71	-23.46 ± 0.07	Ly α	5 ± 1	650 ± 170	42.99 ± 0.06
Candidate Obscured Quasars						
<i>J142322.01 + 020612.8</i>	6.88	-24.28 ± 0.34	Ly α	67 ± 21	< 230	44.33 ± 0.02
<i>J125001.43 + 015243.2</i>	6.29	-21.67 ± 0.62	Ly α	270 ± 150	300 ± 100	43.89 ± 0.02
<i>J131304.72 + 003542.2</i>	6.23	-22.60 ± 0.12	Ly α	120 ± 10	270 ± 10	43.92 ± 0.01
<i>J125456.03 - 005857.9</i>	6.17	-23.30 ± 0.07	Ly α	11 ± 1	< 230	43.14 ± 0.03
<i>J020719.59 + 023826.0</i>	6.14	-20.23 ± 1.59	Ly α	840 ± 830	400 ± 30	44.06 ± 0.01
<i>J022336.97 - 015636.1</i>	6.13	-23.00 ± 0.08	Ly α	51 ± 4	450 ± 70	43.70 ± 0.01
<i>J132535.14 + 012947.2</i>	6.10	-23.44 ± 0.07	Ly α	15 ± 2	330 ± 140	43.34 ± 0.05
<i>J133846.93 - 005339.5</i>	6.09	-22.69 ± 0.20	Ly α	88 ± 17	330 ± 150	43.81 ± 0.02
<i>J131448.69 + 031106.4</i>	6.04	-22.92 ± 0.09	Ly α	36 ± 3	270 ± 30	43.51 ± 0.01
<i>J143905.32 + 032356.0</i>	6.03	-22.77 ± 0.09	Ly α	66 ± 6	240 ± 30	43.72 ± 0.01
<i>J015158.79 + 043325.6</i>	6.01	-23.01 ± 0.16	Ly α	16 ± 3	390 ± 60	43.27 ± 0.03
Galaxies						
<i>J013633.12 + 003410.3</i>	6.28	-23.29 ± 0.08
<i>J100702.44 + 050545.9</i>	6.25	-23.82 ± 0.06
<i>J013958.57 + 034539.5</i>	6.10	-23.25 ± 0.07
<i>J135933.30 + 025909.3</i>	6.09	-23.00 ± 0.11	Ly α	7 ± 1	390 ± 310	42.85 ± 0.08
<i>J233252.97 + 024353.0</i>	6.08	-23.57 ± 0.11
<i>J133605.10 + 022147.1</i>	6.02	-23.23 ± 0.07
<i>J112550.16 - 001619.6</i>	6.01	-24.25 ± 0.30
<i>J140637.84 + 430623.2</i>	5.98	-23.25 ± 0.05	Ly α	1.3 ± 0.4	220 ± 210	42.27 ± 0.12
<i>J140625.39 + 430504.7</i>	5.98	-22.28 ± 0.09	Ly α	6 ± 1	480 ± 160	42.54 ± 0.08
<i>J020213.75 + 011910.1</i>	5.94	-23.01 ± 0.18
<i>J084902.00 - 013025.7</i>	5.94	-23.00 ± 0.12
<i>J235527.98 + 024447.4</i>	5.93	-23.38 ± 0.14
<i>J132746.13 - 015410.3</i>	5.92	-23.38 ± 0.08
<i>J132514.41 + 034006.0</i>	5.92	-23.25 ± 0.06	Ly α	0.8 ± 0.3	< 230	42.05 ± 0.16
<i>J104800.36 + 011856.4</i>	5.91	-23.12 ± 0.15
<i>J021103.93 + 015516.9</i>	5.91	-23.40 ± 0.13
<i>J135059.71 + 023717.3</i>	5.90	-22.74 ± 0.10
<i>J014056.95 - 005048.7</i>	5.89	-23.27 ± 0.07
<i>J131024.32 + 005002.0</i>	5.88	-23.16 ± 0.08
<i>J003554.15 + 030807.3</i>	5.87	-24.27 ± 0.04

Table 1 *continued*

Table 1 (*continued*)

Name	Redshift	M_{1450}	Line	EW_{rest}	FWHM	$\log L_{\text{line}}$
		(mag)		(Å)	(km s $^{-1}$)	(L_{line} in erg s $^{-1}$)
<i>J</i> 120542.50 + 041430.1	5.86	-23.14 ± 0.21
<i>J</i> 103825.94 – 004418.9	5.86	-23.22 ± 0.06
<i>J</i> 124359.28 + 015305.5	5.86	-23.07 ± 0.07
<i>J</i> 000928.93 + 001644.7	5.83	-23.16 ± 0.10
<i>J</i> 234434.18 + 022645.7	5.83	-23.50 ± 0.09
<i>J</i> 123934.04 + 025845.8	5.82	-22.92 ± 0.08	Ly α	4 ± 1	450 ± 70	42.68 ± 0.11
<i>J</i> 000440.93 + 010500.8	5.81	-23.06 ± 0.04
<i>J</i> 113411.21 – 001956.1	5.74	-23.42 ± 0.11
<i>J</i> 145945.34 + 415206.4	5.56	-24.62 ± 0.13
[O III] Emitters						
<i>J</i> 000526.30 – 001247.9	0.955	...	H γ
		...	H β	150 ± 40	< 230	40.90 ± 0.08
		...	[OIII] $\lambda 4959$	450 ± 100	< 230	41.37 ± 0.03
		...	[OIII] $\lambda 5007$	1000 ± 200	< 230	41.73 ± 0.02
<i>J</i> 005743.52 + 044117.4	0.924	...	H γ	170 ± 90	< 230	41.07 ± 0.09
		...	H β	390 ± 190	< 230	41.43 ± 0.03
		...	[OIII] $\lambda 4959$	340 ± 160	< 230	41.37 ± 0.03
		...	[OIII] $\lambda 5007$	2000 ± 900	< 230	42.14 ± 0.01
<i>J</i> 090048.11 – 020909.6	0.855	...	H γ
		...	H β	770 ± 380	< 190	41.62 ± 0.02
		...	[OIII] $\lambda 4959$	1900 ± 900	< 190	42.01 ± 0.01
		...	[OIII] $\lambda 5007$	5900 ± 2900	< 190	42.50 ± 0.01
<i>J</i> 023836.16 – 021027.8	0.792	...	H γ
		...	H β
		...	[OIII] $\lambda 4959$	> 90	< 230	41.177 ± 0.173
		...	[OIII] $\lambda 5007$	> 240	< 230	41.582 ± 0.020
<i>J</i> 020216.24 + 025309.4	0.784	...	H γ
		...	H β	> 70	210 ± 60	41.216 ± 0.098
		...	[OIII] $\lambda 4959$	> 240	< 230	41.735 ± 0.039
		...	[OIII] $\lambda 5007$	> 620	< 230	42.141 ± 0.015

NOTE— The redshifts of quasars, candidate obscured quasars, and galaxies have uncertainties $\Delta z \sim 0.01 - 0.1$, depending on the spectral features around Ly α (e.g., Matsuoka et al. 2022). “EW_{rest}” represents the rest-frame equivalent width; 3 σ lower limits are reported for objects without detectable continuum.

ACKNOWLEDGMENTS

This research is based on data collected at Subaru Telescope, which is operated by the National Astronomical Observatory of Japan. We are honored and grateful for the opportunity of observing the Universe from Maunakea, which has the cultural, historical and natural significance in Hawaii. We appreciate the staff members of the telescope for their support during our FOCAS observations. The data analysis was in part carried out on the open use data analysis computer system at the Astronomy Data Center of NAOJ.

This work is also based on observations made with the GTC, installed at the Spanish Observatorio del Roque de los Muchachos of the Instituto de Astrofísica de Canarias, on the island of La Palma. We thank the support astronomers for their help during preparation and execution of our observing program.

Y. M. was supported by the Japan Society for the Promotion of Science (JSPS) KAKENHI Grant No. 21H04494. K. I. acknowledges the support under the

grant PID2022-136827NB-C44 provided by MCIN/AEI /10.13039/501100011033 / FEDER, EU. M. O was supported by the JSPS KAKENHI Grant No. G24K22894.

The HSC collaboration includes the astronomical communities of Japan and Taiwan, and Princeton University. The HSC instrumentation and software were developed by the National Astronomical Observatory of Japan (NAOJ), the Kavli Institute for the Physics and Mathematics of the Universe (Kavli IPMU), the University of Tokyo, the High Energy Accelerator Research Organization (KEK), the Academia Sinica Institute for Astronomy and Astrophysics in Taiwan (ASIAA), and Princeton University. Funding was contributed by the FIRST program from the Japanese Cabinet Office, the Ministry of Education, Culture, Sports, Science and Technology (MEXT), the Japan Society for the Promotion of Science (JSPS), Japan Science and Technology Agency (JST), the Toray Science Foundation, NAOJ, Kavli IPMU, KEK, ASIAA, and Princeton University.

This paper is based on data retrieved from the HSC data archive system, which is operated by Subaru Telescope and Astronomy Data Center (ADC) at NAOJ. Data analysis was in part carried out with the cooperation of Center for Computational Astrophysics (CfCA) at NAOJ.

This paper makes use of software developed for Vera C. Rubin Observatory. We thank the Rubin Observatory for making their code available as free software at <http://pipelines.lsst.io/>.

The Pan-STARRS1 Surveys (PS1) and the PS1 public science archive have been made possible through contributions by the Institute for Astronomy, the University of Hawaii, the Pan-STARRS Project Office, the Max Planck Society and its participating institutes, the Max Planck Institute for Astronomy, Heidelberg, and the Max Planck Institute for Extraterrestrial Physics, Garching, The Johns Hopkins University, Durham University, the University of Edinburgh, the Queen's University Belfast, the Harvard-Smithsonian Center for Astrophysics, the Las Cumbres Observatory Global Telescope Network Incorporated, the National Central University of Taiwan, the Space Telescope Science Institute, the National Aeronautics and Space Administration under grant No. NNX08AR22G issued through the Planetary Science Division of the NASA Science Mission Directorate, the National Science Foundation grant No. AST-1238877, the University of Maryland, Eotvos Lorand University (ELTE), the Los Alamos National Laboratory, and the Gordon and Betty Moore Foundation.

APPENDIX

We present the journal of spectroscopic observations in Table 2.

Table 2. Journal of Discovery Spectroscopy

Object	i_{AB} (mag)	z_{AB} (mag)	y_{AB} (mag)	t_{exp} (min)	Date (Inst)
Quasars					
<i>J</i> 133013.00 + 423432.2	>26.10	>25.05	22.67 ± 0.05	60	2025 Jan 28 (O)
<i>J</i> 140344.28 + 423114.3	>26.06	>25.04	22.61 ± 0.05	30	2022 Apr 24 (F)
<i>J</i> 225706.60 + 053102.4	>25.68	>25.00	22.72 ± 0.07	60	2024 Sep 25 (O)
<i>J</i> 223942.28 + 040943.2	>26.14	>25.58	23.57 ± 0.09	120	2024 Nov 06 (F)
<i>J</i> 015851.37 + 052410.3	>25.04	25.37 ± 0.79	22.17 ± 0.07	60	2024 Oct 29 (O)
<i>J</i> 142817.13 + 045430.3	25.81 ± 0.32	>24.24	21.26 ± 0.02	60	2025 Jan 24 (O)
<i>J</i> 225810.01 + 035345.3	25.51 ± 0.16	23.38 ± 0.08	20.80 ± 0.01	20	2021 Nov 25 (F)
<i>J</i> 125934.97 + 021309.0	25.52 ± 0.11	22.42 ± 0.03	21.75 ± 0.02	15	2023 Jan 10 (F)
<i>J</i> 113206.98 + 035011.7	27.47 ± 0.74	23.84 ± 0.07	23.44 ± 0.08	40	2022 Dec 13 (F)
<i>J</i> 134014.18 + 025855.0	25.37 ± 0.13	22.22 ± 0.02	21.80 ± 0.02	20	2023 Jan 11 (F)
<i>J</i> 221858.14 + 062406.3	25.64 ± 0.16	22.44 ± 0.04	22.44 ± 0.05	20	2024 Aug 10 (O)

Table 2 *continued*

Table 2 (*continued*)

Object	i_{AB} (mag)	z_{AB} (mag)	y_{AB} (mag)	t_{exp} (min)	Date (Inst)
<i>J132905.06 + 431640.4</i>	26.76 ± 0.35	22.65 ± 0.02	23.17 ± 0.08	20	2022 Dec 27 (F)
<i>J133534.37 + 025702.7</i>	25.87 ± 0.28	22.86 ± 0.03	22.94 ± 0.05	15	2023 Jan 10 (F)
<i>J113007.51 + 051149.1</i>	25.51 ± 0.18	22.22 ± 0.02	21.59 ± 0.02	15	2022 Dec 13 (F)
<i>J094624.10 - 001233.7</i>	>26.27	24.01 ± 0.07	23.87 ± 0.14	30	2022 Dec 13 (F)
<i>J111123.42 + 034039.4</i>	>26.50	23.13 ± 0.02	24.90 ± 0.30	60	2023 Mar 17 (O)
<i>J013603.22 + 022605.0</i>	25.19 ± 0.11	21.61 ± 0.01	21.98 ± 0.02	15	2024 Aug 12 (O)
<i>J023558.20 + 043456.8</i>	25.97 ± 0.32	23.01 ± 0.04	22.99 ± 0.11	45	2024 Sep 13 (O)
<i>J125139.16 + 023342.2</i>	>25.88	22.85 ± 0.03	24.54 ± 0.19	10	2022 Dec 13 (F)
<i>J135818.89 - 013249.7</i>	26.87 ± 0.38	23.66 ± 0.05	24.10 ± 0.20	60	2024 Jul 01 (O)
<i>J133740.18 + 434557.6</i>	26.41 ± 0.30	23.54 ± 0.06	23.34 ± 0.09	30	2022 Dec 26 (F)
<i>J141305.38 + 035829.9</i>	25.88 ± 0.22	23.50 ± 0.06	23.58 ± 0.12	67	2025 Feb 04 (O)
<i>J105642.67 + 041902.1</i>	>26.25	23.85 ± 0.05	25.51 ± 0.68	30	2024 Nov 08 (F)
<i>J020038.83 - 021052.0</i>	>26.04	23.67 ± 0.05	26.49 ± 0.99	20	2021 Nov 25 (F)
<i>J022215.99 - 012534.4</i>	>25.87	23.98 ± 0.06	24.06 ± 0.13	50	2021 Dec 25 (F)
<i>J020236.24 + 030033.6</i>	27.11 ± 0.59	23.87 ± 0.06	23.89 ± 0.19	30	2021 Dec 25 (F)
<i>J131609.75 + 003553.6</i>	26.45 ± 0.34	23.40 ± 0.04	23.28 ± 0.08	60	2023 Mar 17 (O)
<i>J134021.30 + 031939.2</i>	26.21 ± 0.25	23.26 ± 0.04	23.74 ± 0.10	30	2023 Jan 10 (F)
<i>J001705.78 + 004343.3</i>	26.08 ± 0.19	23.35 ± 0.04	24.88 ± 0.40	10	2021 Nov 25 (F)
<i>J015812.02 + 002436.1</i>	25.36 ± 0.11	22.92 ± 0.03	23.46 ± 0.08	15	2021 Nov 27 (F)
<i>J115900.87 + 025819.2</i>	26.53 ± 0.39	23.13 ± 0.04	24.32 ± 0.15	60	2023 Mar 15 (O)
<i>J220754.87 + 065111.8</i>	24.29 ± 0.04	21.59 ± 0.01	22.24 ± 0.05	30	2024 Nov 06 (F)
<i>J011830.06 + 023642.1</i>	25.34 ± 0.13	22.85 ± 0.03	22.81 ± 0.06	15	2021 Nov 27 (F)
<i>J124642.21 + 051048.9</i>	24.53 ± 0.07	21.94 ± 0.02	22.09 ± 0.05	15	2022 Dec 27 (F)
<i>J003658.18 + 034313.2</i>	24.90 ± 0.08	22.86 ± 0.02	23.03 ± 0.05	25	2021 Nov 27 (F)
<i>J131830.28 + 051231.7</i>	24.55 ± 0.07	22.32 ± 0.03	22.16 ± 0.04	25	2023 Jan 10 (F)
<i>J142421.11 + 040512.1</i>	24.16 ± 0.04	21.85 ± 0.01	21.93 ± 0.02	15	2022 May 26 (O)
<i>J023811.54 + 040416.5</i>	24.72 ± 0.18	22.00 ± 0.02	22.08 ± 0.05	15	2024 Sep 13 (O)
<i>J003604.19 + 040912.0</i>	24.94 ± 0.08	23.32 ± 0.04	23.70 ± 0.10	20	2021 Nov 25 (F)
<i>J012031.64 + 004226.7</i>	25.45 ± 0.12	23.45 ± 0.05	23.59 ± 0.08	20	2021 Nov 25 (F)
<i>J130518.55 + 030437.5</i>	23.74 ± 0.02	21.96 ± 0.01	21.97 ± 0.02	30	2023 Jan 11 (F)
<i>J133611.60 - 011929.6</i>	24.70 ± 0.06	22.70 ± 0.02	22.25 ± 0.02	30	2024 Mar 29 (F)
<i>J224357.80 + 061816.1</i>	24.79 ± 0.15	23.25 ± 0.06	23.48 ± 0.15	50	2024 Nov 08 (F)
Candidate Obscured Quasars					
<i>J142322.01 + 020612.8</i>	>26.09	>25.45	23.63 ± 0.08	70	2022 Apr 23 (F)
<i>J125001.43 + 015243.2</i>	>25.92	23.87 ± 0.05	24.86 ± 0.25	60	2023 Mar 17 (O)
<i>J131304.72 + 003542.2</i>	>26.07	23.83 ± 0.07	24.37 ± 0.22	30	2024 Mar 29 (F)
<i>J125456.03 - 005857.9</i>	26.93 ± 0.49	23.92 ± 0.08	24.02 ± 0.19	30	2024 Mar 29 (F)
<i>J020719.59 + 023826.0</i>	>26.00	23.67 ± 0.05	24.95 ± 0.61	15	2021 Nov 26 (F)
<i>J022336.97 - 015636.1</i>	26.02 ± 0.19	23.70 ± 0.04	23.93 ± 0.11	30	2021 Dec 24 (F)
<i>J132535.14 + 012947.2</i>	26.02 ± 0.22	23.59 ± 0.04	23.60 ± 0.08	50	2024 Mar 28 (F)

Table 2 *continued*

Table 2 (*continued*)

Object	i_{AB}	z_{AB}	y_{AB}	t_{exp}	Date (Inst)
	(mag)	(mag)	(mag)	(min)	
<i>J133846.93 – 005339.5</i>	>26.15	23.72 ± 0.05	23.65 ± 0.09	30	2024 Mar 28 (F)
<i>J131448.69 + 031106.4</i>	26.82 ± 0.31	23.78 ± 0.05	23.78 ± 0.10	30	2024 Mar 29 (F)
<i>J143905.32 + 032356.0</i>	26.08 ± 0.23	23.73 ± 0.06	24.21 ± 0.25	30	2024 Mar 30 (F)
<i>J015158.79 + 043325.6</i>	25.82 ± 0.19	23.81 ± 0.07	24.15 ± 0.22	30	2024 Nov 06 (F)
Galaxies					
<i>J013633.12 + 003410.3</i>	>26.03	23.82 ± 0.07	24.17 ± 0.16	25	2021 Nov 26 (F)
<i>J100702.44 + 050545.9</i>	27.22 ± 0.92	23.88 ± 0.11	23.31 ± 0.08	30	2024 Mar 30 (F)
<i>J013958.57 + 034539.5</i>	27.41 ± 0.76	23.86 ± 0.07	23.48 ± 0.11	50	2024 Nov 07 (F)
<i>J135933.30 + 025909.3</i>	27.52 ± 0.75	23.93 ± 0.07	23.71 ± 0.13	50	2023 Jan 10 (F)
<i>J233252.97 + 024353.0</i>	27.52 ± 0.61	23.67 ± 0.07	23.49 ± 0.08	30	2021 Dec 25 (F)
<i>J133605.10 + 022147.1</i>	25.32 ± 0.10	23.21 ± 0.04	23.19 ± 0.06	30	2022 Dec 27 (F)
<i>J112550.16 – 001619.6</i>	26.33 ± 0.22	23.89 ± 0.07	24.11 ± 0.20	80	2025 Mar 21 (O)
<i>J140637.84 + 430623.2</i>	25.70 ± 0.16	23.68 ± 0.06	23.46 ± 0.11	30	2022 Dec 26 (F)
<i>J140625.39 + 430504.7</i>	26.65 ± 0.36	24.34 ± 0.09	24.16 ± 0.20	30	2022 Dec 26 (F)
<i>J020213.75 + 011910.1</i>	25.51 ± 0.14	23.76 ± 0.07	24.33 ± 0.18	30	2021 Dec 25 (F)
<i>J084902.00 – 013025.7</i>	25.29 ± 0.10	23.56 ± 0.04	23.35 ± 0.07	50	2022 Dec 27 (F)
<i>J235527.98 + 024447.4</i>	25.62 ± 0.14	23.76 ± 0.06	23.98 ± 0.14	30	2021 Dec 25 (F)
<i>J132746.13 – 015410.3</i>	25.79 ± 0.28	23.54 ± 0.07	23.66 ± 0.17	30	2024 Mar 29 (F)
<i>J132514.41 + 034006.0</i>	25.92 ± 0.22	23.90 ± 0.07	23.80 ± 0.10	30	2024 Mar 30 (F)
<i>J104800.36 + 011856.4</i>	25.56 ± 0.14	23.62 ± 0.03	23.57 ± 0.10	50	2023 Jan 11 (F)
<i>J021103.93 + 015516.9</i>	25.33 ± 0.09	23.28 ± 0.03	23.20 ± 0.06	30	2024 Nov 08 (F)
<i>J135059.71 + 023717.3</i>	25.99 ± 0.18	23.88 ± 0.05	23.87 ± 0.12	30	2024 Mar 30 (F)
<i>J014056.95 – 005048.7</i>	25.61 ± 0.25	23.54 ± 0.08	23.98 ± 0.15	50	2021 Dec 23 (F)
<i>J131024.32 + 005002.0</i>	27.43 ± 0.69	23.76 ± 0.05	23.65 ± 0.10	50	2024 Mar 28 (F)
<i>J003554.15 + 030807.3</i>	24.11 ± 0.04	22.65 ± 0.02	22.44 ± 0.03	15	2021 Nov 27 (F)
<i>J120542.50 + 041430.1</i>	25.70 ± 0.11	23.69 ± 0.06	24.13 ± 0.16	30	2022 Dec 13 (F)
<i>J103825.94 – 004418.9</i>	26.21 ± 0.20	23.82 ± 0.04	23.66 ± 0.08	30	2024 Mar 29 (F)
<i>J124359.28 + 015305.5</i>	25.86 ± 0.33	23.78 ± 0.05	23.80 ± 0.10	30	2024 Mar 30 (F)
<i>J000928.93 + 001644.7</i>	25.32 ± 0.09	23.75 ± 0.06	23.93 ± 0.12	30	2021 Dec 25 (F)
<i>J234434.18 + 022645.7</i>	24.97 ± 0.08	23.36 ± 0.04	23.53 ± 0.10	30	2024 Nov 07 (F)
<i>J123934.04 + 025845.8</i>	25.99 ± 0.23	23.88 ± 0.05	23.85 ± 0.08	30	2024 Mar 30 (F)
<i>J000440.93 + 010500.8</i>	25.35 ± 0.09	23.73 ± 0.05	23.70 ± 0.09	30	2021 Nov 27 (F)
<i>J113411.21 – 001956.1</i>	25.33 ± 0.09	23.63 ± 0.05	24.24 ± 0.18	60	2024 Apr 03 (O)
<i>J145945.34 + 415206.4</i>	23.85 ± 0.08	22.34 ± 0.04	22.56 ± 0.07	15	2024 Apr 13 (O)
[O III] Emitters					
<i>J000526.30 – 001247.9</i>	25.42 ± 0.10	26.36 ± 0.54	23.61 ± 0.09	20	2021 Dec 24 (F)
<i>J005743.52 + 044117.4</i>	25.20 ± 0.14	>25.13	23.54 ± 0.09	10	2021 Dec 24 (F)
<i>J090048.11 – 020909.6</i>	24.05 ± 0.06	22.52 ± 0.03	23.27 ± 0.13	30	2024 Oct 22 (O)
<i>J023836.16 – 021027.8</i>	25.82 ± 0.62	23.68 ± 0.09	24.96 ± 0.58	20	2021 Dec 26 (F)
<i>J020216.24 + 025309.4</i>	26.34 ± 0.29	23.91 ± 0.08	24.72 ± 0.38	10	2021 Dec 24 (F)

Table 2 *continued*

Table 2 (*continued*)

Object	i_{AB} (mag)	z_{AB} (mag)	y_{AB} (mag)	t_{exp} (min)	Date (Inst)
Brown Dwarfs					
<i>J</i> 002006.91 + 021707.3	24.48 ± 0.05	22.90 ± 0.04	22.83 ± 0.07	45	2024 Aug 10 (O)
<i>J</i> 004314.13 + 051600.4	23.98 ± 0.06	22.46 ± 0.03	22.60 ± 0.09	20	2024 Sep 06 (O)
<i>J</i> 004604.07 + 032818.6	25.04 ± 0.08	23.76 ± 0.05	23.31 ± 0.06	30	2021 Nov 25 (F)
<i>J</i> 005534.96 + 051051.0	25.57 ± 0.21	22.67 ± 0.02	21.90 ± 0.03	35	2024 Aug 12 (O)
<i>J</i> 011926.03 + 035801.2	24.89 ± 0.10	23.29 ± 0.07	23.38 ± 0.13	120	2024 Sep 06 (O)
<i>J</i> 013834.04 + 031801.3	24.79 ± 0.07	23.84 ± 0.07	23.36 ± 0.11	20	2021 Nov 26 (F)
<i>J</i> 014653.54 + 043154.6	24.93 ± 0.13	23.33 ± 0.08	23.44 ± 0.13	120	2024 Sep 07 (O)
<i>J</i> 015507.67 + 034557.2	25.24 ± 0.04	23.26 ± 0.05	23.09 ± 0.11	60	2024 Sep 11 (O)
<i>J</i> 021331.56 – 021215.3	25.24 ± 0.16	23.78 ± 0.07	23.36 ± 0.07	40	2021 Nov 26,27 (F)
<i>J</i> 022330.97 + 000216.7	24.72 ± 0.05	23.13 ± 0.04	23.06 ± 0.07	60	2024 Sep 15 (O)
<i>J</i> 023549.99 – 001719.5	24.45 ± 0.05	22.40 ± 0.04	22.30 ± 0.05	20	2024 Aug 12 (O)
<i>J</i> 083814.13 + 013741.8	26.78 ± 0.36	23.77 ± 0.04	22.75 ± 0.03	40	2021 Dec 24 (F)
<i>J</i> 084007.89 + 051351.7	>25.04	22.74 ± 0.07	21.92 ± 0.06	20	2024 Nov 06 (F)
<i>J</i> 084427.33 + 022508.0	26.00 ± 0.22	23.21 ± 0.04	22.20 ± 0.02	70	2021 Dec 23,24 (F)
<i>J</i> 092701.24 – 012812.0	27.09 ± 0.63	23.65 ± 0.10	22.97 ± 0.07	40	2024 Nov 06 (F)
<i>J</i> 102059.04 + 030252.2	25.41 ± 0.12	23.20 ± 0.04	22.65 ± 0.05	40	2024 Nov 07 (F)
<i>J</i> 110813.13 + 012353.8	24.89 ± 0.06	23.18 ± 0.04	22.93 ± 0.06	40	2024 Nov 07 (F)
<i>J</i> 110931.21 + 004900.2	25.25 ± 0.09	23.58 ± 0.03	23.29 ± 0.08	60	2024 Mar 15 (O)
<i>J</i> 114838.82 – 021153.5	24.61 ± 0.08	22.16 ± 0.02	21.21 ± 0.02	30	2023 Mar 18 (O)
<i>J</i> 133642.85 + 435628.7	26.79 ± 0.38	25.79 ± 0.42	21.76 ± 0.02	30	2022 Apr 24 (F)
<i>J</i> 140416.94 + 045001.5	25.53 ± 0.14	22.85 ± 0.05	21.79 ± 0.03	60	2025 Mar 22 (O)
<i>J</i> 141220.77 – 012001.0	27.43 ± 0.53	26.05 ± 0.37	23.85 ± 0.09	50	2022 Dec 26 (F)
<i>J</i> 220451.87 + 063342.3	>26.05	>24.55	22.13 ± 0.05	60	2024 Sep 06 (O)
<i>J</i> 220627.21 + 064136.4	23.76 ± 0.07	22.26 ± 0.06	22.39 ± 0.14	16	2024 Aug 10 (O)
<i>J</i> 221336.02 – 000333.2	24.54 ± 0.05	21.69 ± 0.01	20.66 ± 0.01	30	2024 Aug 10 (O)
<i>J</i> 221753.95 + 002342.3	26.72 ± 0.29	25.12 ± 0.22	23.25 ± 0.05	50	2021 Nov 27 (F)
<i>J</i> 222736.05 + 042920.1	>25.94	25.13 ± 0.24	22.94 ± 0.06	30	2021 Nov 26 (F)
<i>J</i> 224011.93 – 012705.4	26.84 ± 0.75	22.52 ± 0.02	21.71 ± 0.04	60	2024 Oct 31 (O)
<i>J</i> 224336.11 + 031740.5	26.81 ± 0.60	25.00 ± 0.22	22.95 ± 0.09	40	2021 Nov 26 (F)
<i>J</i> 234812.70 + 053951.8	24.42 ± 0.13	22.83 ± 0.06	23.21 ± 0.15	45	2024 Sep 13 (O)
Passive galaxies					
<i>J</i> 004219.46 + 045530.1	24.54 ± 0.07	22.84 ± 0.07	23.66 ± 0.13	50	2024 Nov 08 (F)
<i>J</i> 004314.81 + 051632.5	25.10 ± 0.16	23.12 ± 0.07	23.01 ± 0.09	30	2024 Nov 08 (F)
<i>J</i> 011354.43 + 060446.8	24.50 ± 0.13	22.81 ± 0.06	22.64 ± 0.08	50	2024 Nov 09 (F)
<i>J</i> 011949.18 + 055925.0	24.34 ± 0.07	22.75 ± 0.05	22.67 ± 0.07	30	2024 Nov 06 (F)
<i>J</i> 012148.05 + 053026.6	24.72 ± 0.08	23.21 ± 0.06	23.19 ± 0.09	40	2024 Nov 09 (F)
<i>J</i> 012251.39 + 045000.0	24.83 ± 0.07	23.33 ± 0.06	23.36 ± 0.08	40	2024 Nov 09 (F)
<i>J</i> 012703.23 + 055558.9	24.63 ± 0.10	23.07 ± 0.06	23.04 ± 0.09	30	2024 Nov 08 (F)
<i>J</i> 012300.92 + 024904.0	24.51 ± 0.06	23.19 ± 0.04	22.86 ± 0.06	40	2021 Dec 23 (F)

Table 2 *continued*

Table 2 (*continued*)

Object	i_{AB}	z_{AB}	y_{AB}	t_{exp}	Date (Inst)
	(mag)	(mag)	(mag)	(min)	
<i>J</i> 012821.85 + 040331.3	24.60 ± 0.06	23.50 ± 0.05	23.18 ± 0.08	60	2024 Aug 13 (O)
<i>J</i> 104110.52 + 033845.3	>26.11	25.17 ± 0.19	22.79 ± 0.08	30	2022 Dec 13 (F)
<i>J</i> 121643.52 + 043806.1	26.68 ± 0.32	23.66 ± 0.08	23.16 ± 0.08	50	2024 Mar 28 (F)
<i>J</i> 144147.28 + 042329.5	23.58 ± 0.02	21.97 ± 0.02	22.37 ± 0.04	15	2024 Jun 30 (O)
<i>J</i> 162307.07 + 421418.4	24.35 ± 0.04	22.85 ± 0.04	22.68 ± 0.05	30	2024 Apr 13 (O)
<i>J</i> 220252.90 + 065600.4	24.54 ± 0.07	22.99 ± 0.06	23.05 ± 0.13	50	2024 Nov 08 (F)

NOTE—Coordinates are at J2000.0, and magnitude lower limits are placed at 5σ significance. All magnitudes were taken from the HSC-SSP S23B DR, and were corrected for Galactic extinction. The instrument (Inst) “F” and “O” denote Subaru/FOCAS and GTC/OSIRIS, respectively.

REFERENCES

- Aihara, H., Arimoto, N., Armstrong, R., et al. 2018, PASJ, 70, S4. doi:10.1093/pasj/psx066
- Burgasser, A. J. 2014, Astronomical Society of India Conference Series, 11, 7. doi:10.48550/arXiv.1406.4887
- Cepa, J., Aguiar, M., Escalera, V. G., et al. 2000, Proc. SPIE, 4008, 623. doi:10.1117/12.395520
- Coleman, G. D., Wu, C.-C., & Weedman, D. W. 1980, ApJS, 43, 393. doi:10.1086/190674
- Ding, X., Onoue, M., Silverman, J. D., et al. 2025, arXiv:2505.03876. doi:10.48550/arXiv.2505.03876
- Ding, X., Onoue, M., Silverman, J. D., et al. 2023, Nature, 621, 51. doi:10.1038/s41586-023-06345-5
- Euclid Collaboration, Barnett, R., Warren, S. J., et al. 2019, A&A, 631, A85. doi:10.1051/0004-6361/201936427
- Greene, J. E., Labbe, I., Goulding, A. D., et al. 2024, ApJ, 964, 39. doi:10.3847/1538-4357/ad1e5f
- Harikane, Y., Zhang, Y., Nakajima, K., et al. 2023, ApJ, 959, 39. doi:10.3847/1538-4357/ad029e
- Iwamoto, R., Matsuoka, Y., Imanishi, M., et al. 2025, ApJ, 979, 183. doi:10.3847/1538-4357/ada27b
- Izumi, T., Matsuoka, Y., Fujimoto, S., et al. 2021, ApJ, 914, 36. doi:10.3847/1538-4357/abf6dc
- Izumi, T., Onoue, M., Matsuoka, Y., et al. 2021, ApJ, 908, 235. doi:10.3847/1538-4357/abdf7ef
- Izumi, T., Onoue, M., Matsuoka, Y., et al. 2019, PASJ, 71, 111. doi:10.1093/pasj/psz096
- Izumi, T., Onoue, M., Shirakata, H., et al. 2018, PASJ, 70, 36. doi:10.1093/pasj/psy026
- Kashikawa, N., Aoki, K., Asai, R., et al. 2002, PASJ, 54, 6, 819. doi:10.1093/pasj/54.6.819
- Kato, N., Matsuoka, Y., Onoue, M., et al. 2020, PASJ, 72, 84. doi:10.1093/pasj/pssaa074
- Kocevski, D. D., Finkelstein, S. L., Barro, G., et al. 2025, ApJ, 986, 2, 126. doi:10.3847/1538-4357/adbc7d
- Kocevski, D. D., Onoue, M., Inayoshi, K., et al. 2023, ApJL, 954, L4. doi:10.3847/2041-8213/ace5a0
- Konno, A., Ouchi, M., Nakajima, K., et al. 2016, ApJ, 823, 1, 20. doi:10.3847/0004-637X/823/1/20
- Matsuoka, Y., Iwasawa, K., Onoue, M., et al. 2018a, ApJS, 237, 5
- Matsuoka, Y., Iwasawa, K., Onoue, M., et al. 2019, ApJ, 883, 183. doi:10.3847/1538-4357/ab3c60
- Matsuoka, Y., Iwasawa, K., Onoue, M., et al. 2022, ApJS, 259, 18. doi:10.3847/1538-4365/ac3d31
- Matsuoka, Y., Izumi, T., Onoue, M., et al. 2024, ApJL, 965, L4. doi:10.3847/2041-8213/ad35c7
- Matsuoka, Y., Kawara, K., & Oyabu, S. 2008, ApJ, 673, 62. doi:10.1086/524193
- Matsuoka, Y., Onoue, M., Iwasawa, K., et al. 2025, , arXiv:2505.04825. doi:10.48550/arXiv.2505.04825
- Matsuoka, Y., Onoue, M., Iwasawa, K., et al. 2023, ApJL, 949, L42. doi:10.3847/2041-8213/acd69f
- Matsuoka, Y., Onoue, M., Kashikawa, N., et al. 2016, ApJ, 828, 26
- Matsuoka, Y., Onoue, M., Kashikawa, N., et al. 2018b, PASJ, 70, S35
- Matsuoka, Y., Onoue, M., Kashikawa, N., et al. 2019, ApJL, 872, L2. doi:10.3847/2041-8213/ab0216
- Matsuoka, Y., Oyabu, S., Tsuzuki, Y., et al. 2007, ApJ, 663, 781. doi:10.1086/518399
- Matsuoka, Y., Strauss, M. A., Kashikawa, N., et al. 2018c, ApJ, 869, 150
- Matthee, J., Naidu, R. P., Brammer, G., et al. 2024, ApJ, 963, 129. doi:10.3847/1538-4357/ad2345

- Miyazaki, S., Komiyama, Y., Kawanomoto, S., et al. 2018, PASJ, 70, S1. doi:10.1093/pasj/psx063
- Mortlock, D. J., Patel, M., Warren, S. J., et al. 2012, MNRAS, 419, 1, 390. doi:10.1111/j.1365-2966.2011.19710.x
- Oke, J. B. & Gunn, J. E. 1983, ApJ, 266, 713. doi:10.1086/160817
- Onoue, M., Ding, X., Silverman, J. D., et al. 2024, arXiv:2409.07113. doi:10.48550/arXiv.2409.07113
- Onoue, M., Inayoshi, K., Ding, X., et al. 2023, ApJL, 942, L17. doi:10.3847/2041-8213/aca9d3
- Onoue, M., Kashikawa, N., Matsuoka, Y., et al. 2019, ApJ, 880, 77. doi:10.3847/1538-4357/ab29e9
- Onoue, M., Matsuoka, Y., Kashikawa, N., et al. 2021, ApJ, 919, 61. doi:10.3847/1538-4357/ac0f07
- Rigby, J., Perrin, M., McElwain, M., et al. 2023, PASP, 135, 1046, 048001. doi:10.1088/1538-3873/acb293
- Sawamura, M., Izumi, T., Nakanishi, K., et al. 2025, ApJ, 980, 121. doi:10.3847/1538-4357/ada943
- Schlegel, D. J., Finkbeiner, D. P., & Davis, M. 1998, ApJ, 500, 2, 525. doi:10.1086/305772
- Skrzypek, N., Warren, S. J., Faherty, J. K., et al. 2015, A&A, 574, A78. doi:10.1051/0004-6361/201424570
- Sobral, D., Matthee, J., Darvish, B., et al. 2018, MNRAS, 477, 2, 2817. doi:10.1093/mnras/sty782
- Spinosa, D., Orsi, A., López-Sanjuan, C., et al. 2020, A&A, 643, A149. doi:10.1051/0004-6361/202038756
- Takahashi, A., Matsuoka, Y., Onoue, M., et al. 2024, ApJ, 960, 112. doi:10.3847/1538-4357/ad045e
- Toshikawa, J., Kashikawa, N., Ota, K., et al. 2012, ApJ, 750, 2, 137. doi:10.1088/0004-637X/750/2/137